Journal of Nepal Geological Society, 2025, Vol. 69, pp. 97-108
https://doi.org/10.3126/jngs.v69i1.88325

Study on ground deformation in Kathmandu valley using c-band Sentinel-1a synthetic aperture radar (SAR) satellite images

Nabin Sah[1], Kuber Saud[1], *Binod Adhikari[1] and Chali Idosa[2]

[1]Department of Physics, St. Xavier's College, Maitighar, Kathmandu, Nepal.
[2]Department of Physics, College of Natural Sciences, Jimma University, Jimma, 378, Oromia, Ethiopia.
**Corresponding author's email: binod.adhi@gmail.com*

ABSTRACT

Interferometric synthetic aperture radar (InSAR) is a prominent and widely used remote sensing method used for accurate surface deformation across large areas. We applied this technique to study the subsidence and upliftment of the ground surface in Kathmandu Valley in the years between 2019 and 2023 AD. C-band Sentinel-1A images from 2019 to 2023 were employed in this study to investigate the status of ground deformation. This study highlights ground upliftment in major parts of the valley in the year 2022 and 2023 whereas the valley experienced major subsidence during the year 2020 to 2022. These results in agreement with prior studies of tectonic and anthropogenic influences suggest that ongoing tectonic compression combined with intensive groundwater withdrawal have driven the observed patterns. Because the valley lies deep, soft sedimentary fill even moderate ground motions pose hazards to infrastructure. We conclude that Kathmandu's ground is actively deforming and recommend enhanced water resource management and land use planning to mitigate future subsidence risk. In this study we also found that the major subsidence was found in the central north region and southeastern part of the valley. But in the years between 2022 and 2023 major uplifting was found in the northern part of the valley. In general, the study shows major deformation over a four-year time interval which may have occurred due to the seismic movement or groundwater depletion.

Keywords: Interferometric synthetic aperture radar (InSAR); Sentinel -1; Ground deformation; Remote sensing

Received: 25 January 2025 **Accepted:** 12 December 2025

INTRODUCTION

The sluggish settling that is subsidence or elevation of the Earth's surface caused by the underlying movement of Earth components is referred to as ground deformation (Wang et al. 2019). Natural or human processes like subsurface water loss or long run drought and urban development cause ground deformation (Stramondo et al. 2008). Ground deformation often alters topographic gradients resulting in infrastructure damage, land surface rupturing, aggravated floods, inundation of land and decreased reduced aquifer capacity which could end up endangering society and the economy (Holzer and Galloway, 2005). In general the ground distortions caused by underground water extraction have been documented all around the world (Taylor et al. 2013). However, ground deformation produced by manmade constructions is rarely seen (Castellazzi et al. 2016).

Kathmandu has two major land forms alluvial and flood plains that make the valley prone to deforming even more (Bhattarai et al. 2017). The natural factors of ground deformation is an earthquake, volcanic eruptions and others. A large earthquake of Mw 7.8 that occurred on 25 April 2015 occurred along the Main Himalayan Thrust fault in central Nepal. The collision of the Indian Plate beneath the Eurasian Plate was the main reason for the earthquake. Gorkha region was measured as the epicenter which is around 80 km northwest of Kathmandu, and the wave propagated towards the east from the epicenter region passing through the sediment filled Kathmandu Valley. Over 8000 people died as a result of this incident largely in Kathmandu and the surrounding areas (Goda et al. 2015). It is thought that the Himalayan mountain range which was created when the Indian and Eurasian plates collided is an earthquake prone area (M. R. Pandey et al. 1999).

The Indian Plate under thrusts the Eurasian Plate in this region which causes a number of large earthquakes to occur in the Himalayas (Goda et al. 2015). Another factor of ground deformation in Kathmandu Valley is uneven distribution of underground water since the early 1970s (Bhattarai et al. 2017). Groundwater has always been an important source of water in the Kathmandu Valley. In response to the water shortage both governmental and private organizations began to pump groundwater through Individual wells and deep boreholes (Pandey et al. 2012). The location of boreholes in Kathmandu Valley is shown in Fig. 1. In the middle of the 1980s, when the Nepal Water Delivery Corporation began incorporating underground water into its delivery system noticeable effects on water levels were noticed (Chapagain, 2013). During the past decades rapid urbanization has increased the risk of ground deformation in Kathmandu, Nepal (Kumar et al. 2022).

InSAR technology has been used by many researchers since its introduction from microwave remote sensing in the 1950s and has become a scientifically effective method of Earth observation with correspondingly great achievements (Du, Li,

Zhou, et al. 2021). Compared with traditional optical remote sensing the advantage of InSAR technology is its ability to acquire data comparatively less impacted by weather and also phase information from ground objects (Du, Li, Zhou, et al. 2021). InSAR is a mapping technology that employs radar images of the Earth's surface taken by orbiting satellites to record ground deformation. When an object moves towards or away from the satellite the distance traveled by the radar wave varies. This is detected by InSAR as a change in the phase of the returning signal (Zhang et al. 2021).

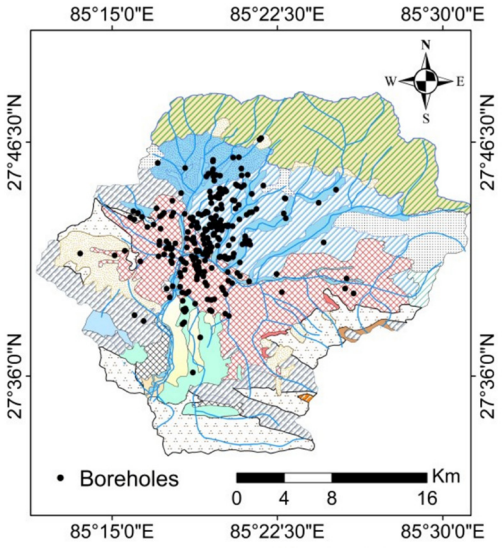

Fig. 1: Mapping of Geological formation of Kathmandu valley with borehole locations (Subedi et al. 2021).

The study of the ground deformation of the Kathmandu Valley was also done during the earthquake in 2015 by taking the pre earthquake and post-earthquake data (Kumar et al. 2022). Their study resulted in serious damage to the whole built-up area with intensities ranging from 1 cm to 23 cm. It showed severe mild deformation/displacement (- 40cm to + 5cm) from north to south roughly following the alignment of Himalayan peaks and valleys in Kathmandu and its neighboring regions. The majority of the regions in central Kathmandu had high subsidence - (10 - 15) cm whereas low subsidence (<5cm) was observed in the northern part of Valley which may have been due to the recent earthquake (Kumar et al. 2022). Overall subsidence in the southern portion of the valley was (>10cm) and considerable subsidence of (>15cm) was seen in the south-eastern and south-western portions. The northern and north-eastern portions of the valley had similar little subsidence of (<5cm) (Kumar et al. 2022). The structural alignments in the Himalayan region which are most likely driven by latitudinal patterns of deformation from north to south were highlighted in their study. Also, their study clarifies the potential use of InSAR technology which can be used in estimating earthquake-induced damage studies at the urban scale and hazard risk assessments that support the development of an efficient disaster risk reduction policy framework for the area.

InSAR with multiple satellite/multiple angle combination technique allows distinguishing and tracking the temporal evolution of three-dimensional (3-D) components of the Earth's surface deformation which were investigated by (Pepe and Calò, 2017). Their research aims to shed light on the multi pass InSAR techniques and their ability for capturing a diverse range of deformation processes.

In this study, we used InSAR technology to look for ground deformation in the Kathmandu Valley. In this study a four-year time span from 2019 to 2023 sees annual observations of earth deformation. The study helps us in understanding the ground deformation features across the Kathmandu Valley between 2019 and 2023.

MATERIALS AND METHODOLOGY

In this research, the following three subtitles were explained under the section Materials and Methodology.

Study area

Kathmandu valley which spans an area of 654.7 km^2 is situated between latitudes 27.34033 and 27.4904 N and longitudes 85.11019 and 85.34057 E (Bajracharya et al. 2015). The valley is home to three important cities: Kathmandu, Bhaktapur and Lalitpur. Around 20,288 people live in the city per square kilometer which equates to 52,550 people per square mile. The average elevation of Kathmandu Valley is roughly 1400 meters above sea level. The valley contains a thick layer of lacustrine and river sediments that extends for more than 550 meters. (M. R. Pandey, 2000). The Geology of the Kathmandu Valley: The Shivapuri Mountain Range is to the north of the valley at 2732 meters, the Phulchauki Mountain Range is to the south at 2762 meters, the Nagarkot Mountain Range is to the east at 1895 meters, and the Chandragiri Mountain Range is to the west at 2356 meters (Piya et al. 2004). The Kathmandu Valley's primary geological components are basement rock and quaternary sediment (Gautam and Rao, 1991). Precambrian to Devonian rocks are primarily sedimentary rock made of calcium carbonate, dolomite, slate, marble, schist, and garnet schist are what create the basement rock of the valley (Moribayashi and Maruo, 1980). The quaternary deposit was composed of 650m of thick deep semi consolidated fluvial lacustrine layers. It is composed of sand and gravel with fine to coarse-grained sedimentary rocks. (Piya et al. 2004).

Data

The open access Sentinel-1A data is used to monitor the ground deformation of Kathmandu Valley. The Sentinel -1 Satellite obtains global images in IW (Interferometric wide) mode with routine acquisition ability. The Sentinel-1 IW images have a spatial resolution of 5 m in range and 20 m in azimuth (Du, Li, Chen, et al. 2021). The Twin polar orbiting satellites on the Sentinel-1 are equipped to supply geographical data for environmental and security warranting as well as for the expansion of the world economy and business. The satellite's function both during the day and at night and performs a synthetic aperture with radar imaging. We can obtain imagery using Sentinel-1 bands in any weather. An active phased array antenna called C-SAR was developed to offer faster azimuth and elevation scanning. It allows to cover bigger areas of

incidence angle to support the scan SAR operation (Yulianto et al. 2021). In this research Interferometric Wide (IW) SAR images from the Sentinel-1 satellites were downloaded in Single Look Complex (SLC) format through Open Access Hub (Copernicus.eu). Images were downloaded annually for the measurement of ground deformation from the year 2019 to 2023 with VV polarization generally meaning the transmitter and recovery are aligned vertically.

With a 6-day repeat cycle and 175 orbits each cycle, Sentinel-1 is in a sun synchronous near polar orbit. Both Sentinel-1A and Sentinel-1B share the same orbit plain with a 180-orbital phasing difference. The orbit altitude of Sentinel 1 Satellite is 693 km (Yulianto et al. 2021). Parameters of the images used in this study are shown in table 1.

Methodology

We applied Differential InSAR to each consecutive-year image pair (2019-2020, 2020-2021, etc.) using ESA's SNAP toolbox and standard procedures. The main steps were: (1) Co-registration: Align each slave image to the master image using precise orbital information ensuring sub-pixel accuracy. (2) Interferogram Formation: Multiply the master SLC by the conjugate of the slave to form a wrapped phase interferogram. (3) Topographic Phase Removal: Use the DEM to subtract the phase due to topography and isolating residual phase caused by displacement, atmospheric delay and noise. (4) Filtering and Multi-looking: Apply a Goldstein or similar adaptive filter and multi-looking (spatial averaging) to reduce phase noise and improve coherence. (5) Phase Unwrapping: Convert the filtered wrapped phase to a continuous phase field using the SNAPHU algorithm. (6) Displacement Conversion: Convert unwrapped phase to line-of-sight (LOS) displacement using the radar wavelength and incidence angle. (7) Geocoding: Project the LOS displacement map to geographic coordinates. A pair of interferometry data can have a phase difference, which can be written as follows using Equation 1 and InSAR phase can be modeled as

$\varphi\_int = \varphi\_disp + \varphi\_atm + \varphi\_noise + \varphi\_topo + \varphi\_flat$ (Bhattarai et al. 2017) .....(1)

where φ_disp is the phase due to ground movement, φ_topo is known from the DEM and φ_flat accounts for ideal Earth reference. By removing φ_topo and correcting orbits the remaining phase is assumed to represent mostly φ_disp (plus minor atmospheric/noise terms). We took the DEM corrected interferogram and unwrapped it to obtain the cumulative LOS displacement between the two acquisition dates for each pair. The overall workflow is depicted in Fig. 3 (flowchart) and matches standard DInSAR methodology (Bhattarai et al. 2017).

Table 1: Parameter of images used for the study

Acquisition data	Frequency	Polarization	Orbit number start	Orbit number End	Product type	Spatial resolution	mode
2019/01/06	c-band	VV	25375	25375	SLC	5x5 m	Iw
2020/01/01	c-band	VV	30607	30607	SLC	5x5 m	Iw
2021/01/07	c-band	VV	36032	36032	SLC	5x5 m	Iw
2022/01/02	c-band	VV	41282	41282	SLC	5x5 m	Iw
2023/01/09	c-band	VV	46707	46707	SLC	5x5 m	Iw

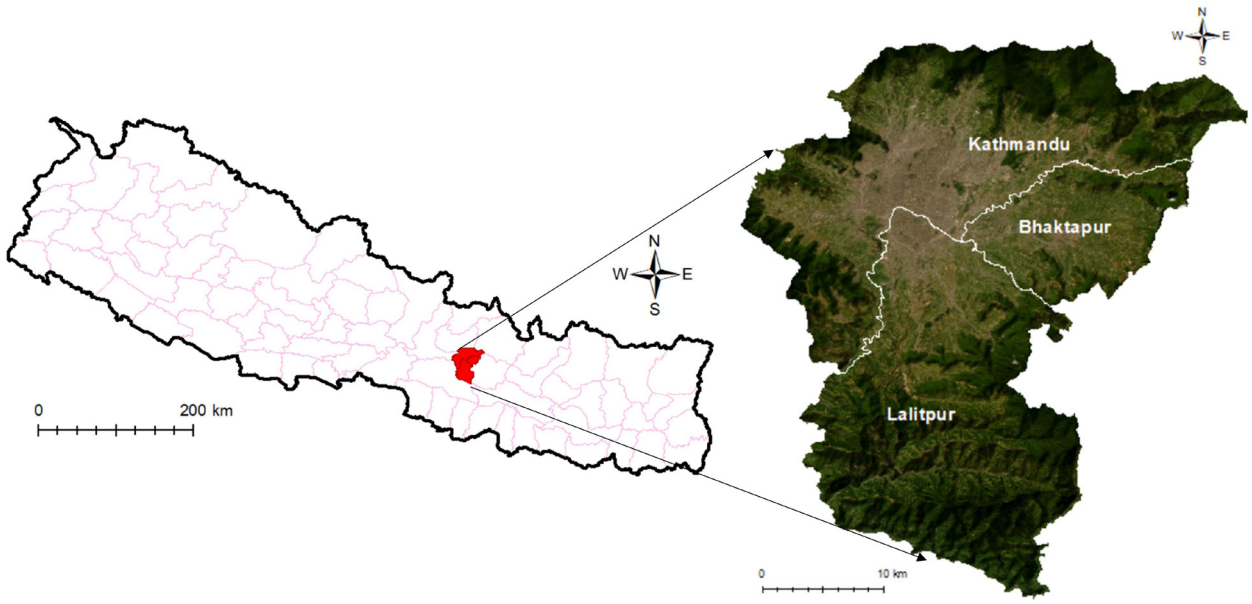

Fig. 2: Map of Kathmandu valley showing Kathmandu, Bhaktapur and Lalitpur districts.

We used Snap toolbox for the processing of the images obtained from Sentinel-1 satellite and the overall workflow of the sentinel-1 InSAR processing through the snap toolbox for ground surface deformation.

RESULT

We generated LOS displacement maps for each annual interval (2019-2020, 2020-2021, 2021-2022, 2022-2023). This study attempts to track the ground deformation of the Kathmandu Valley in years between 2019 and 2023 along with their deformation in one-year time intervals. Overall, five satellite image data were used to monitor the deformation pattern. A total of four combination was use for the study and the SAR combination that were used is shown in the Fig. 6 and the output images after processing are shown in Figs. 7,8,9 and 10.

The four main interferometric maps (2019-2020, 2020-2021, 2021-2022 and 2022-2023) provide the spatial backbone for our analysis and were produced from four Sentinel-1A SLC combinations as shown in Fig. 4. Each map was generated following the SNAP workflow described in Section 2.3 and was geocoded to the Kathmandu Valley extent and the colors are scaled so that cool tones indicate LOS subsidence and warm tones indicate LOS.

Visual comparison of the four annual maps shows a clear basin scale temporal evolution and widespread subsidence dominate the first three intervals while an overall uplift signal appears in 2022-2023. The map series therefore suggests a transient multi-year process rather than a spatially fixed deformation pattern. This sequence motivates the site-by-site quantification summarized in Table 2 and Table 3 which are referenced routinely below.

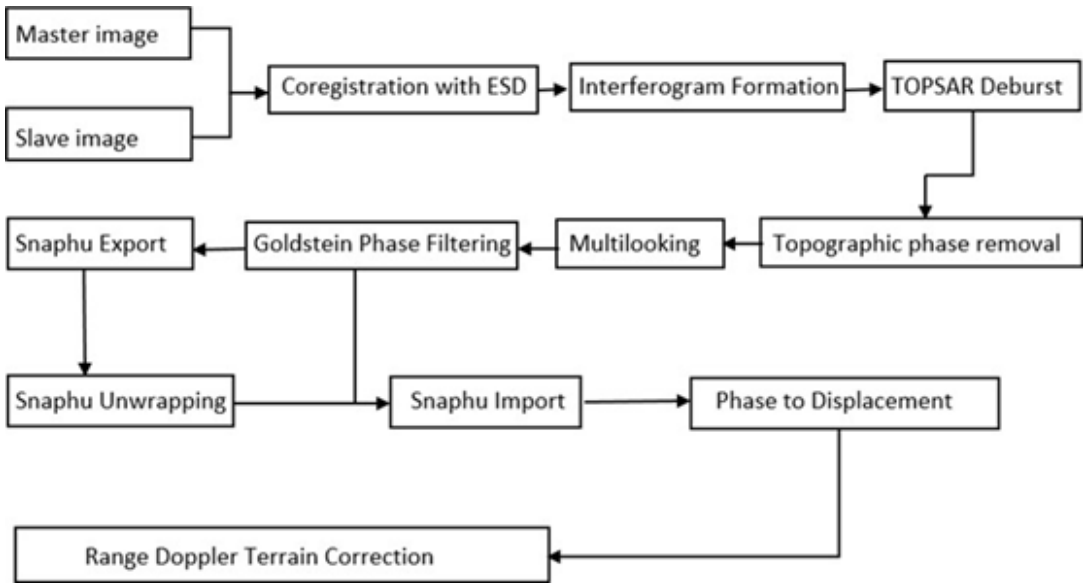

Fig. 3: A systematic flowchart of methodology.

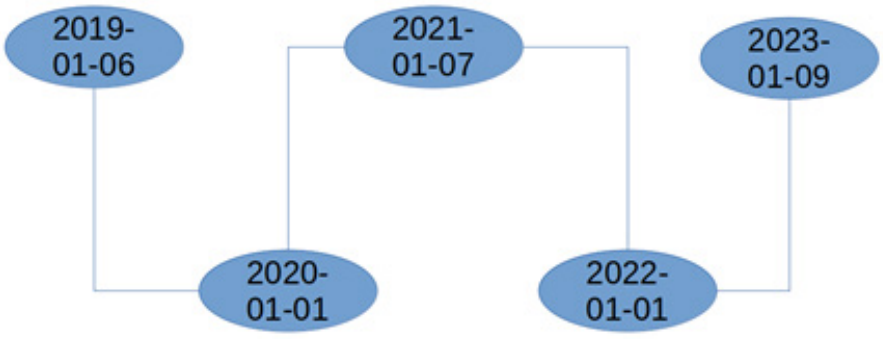

Fig. 4: Sentinel 1 image combination use for data processing. Overall, four combination was made with one combination having two-year image

On the 2019-2020 map as shown in the Fig. 5 the dominant signal is negative i.e. subsidence across much of the basin floor with a few peripherals showing modest positive values. Also, Table 2 reports representative ranges for central locations like Thamel shows -5.5 to -8.5 cm for 2019-2020, New Baneshwor -4 to -8 cm and Lagankhel -2 to -5 cm. The corresponding histogram for that interval in Fig. 09 left reinforces the predominance of downward bars relative to the zero reference line hence indicating that more sites subsided than uplifted during this year pair. The spatial pattern strongest subsidence in central which is densely urbanized districts is consistent with expected anthropogenic stress on shallow aquifers and with earlier InSAR findings in Kathmandu(Bhattarai et al. 2017). These numeric and spatial observations form the baseline for the subsequent intensification observed in 2020-2021.

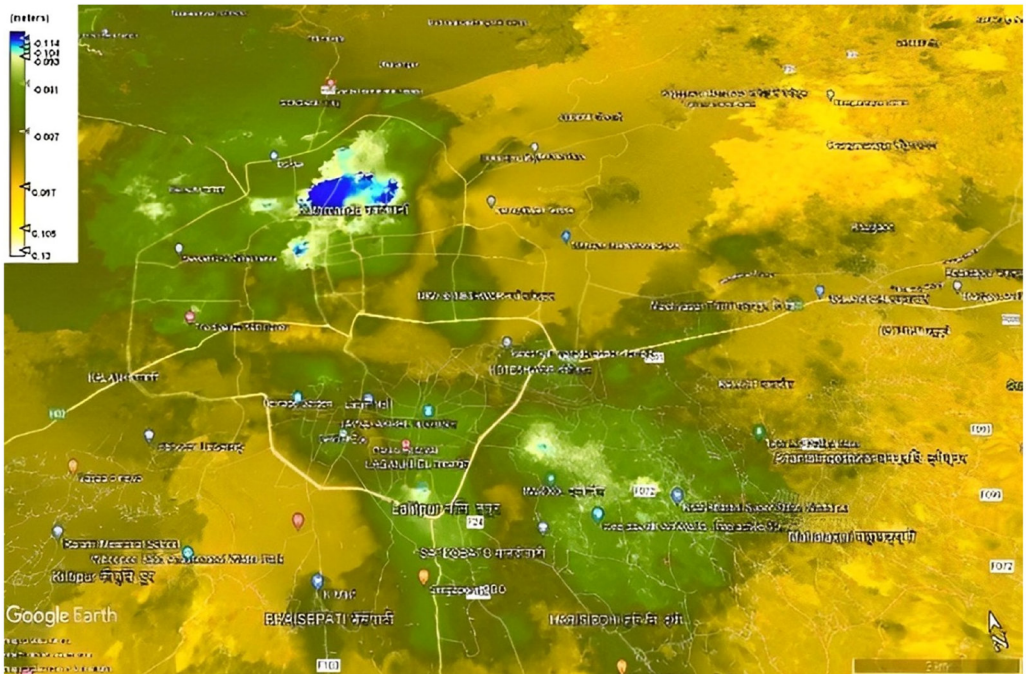

Fig. 5: Map of ground displacement over Kathmandu Valley in the year 2019-2020. The white and yellow part represents maximum ground upliftment and blue represents subsidence.

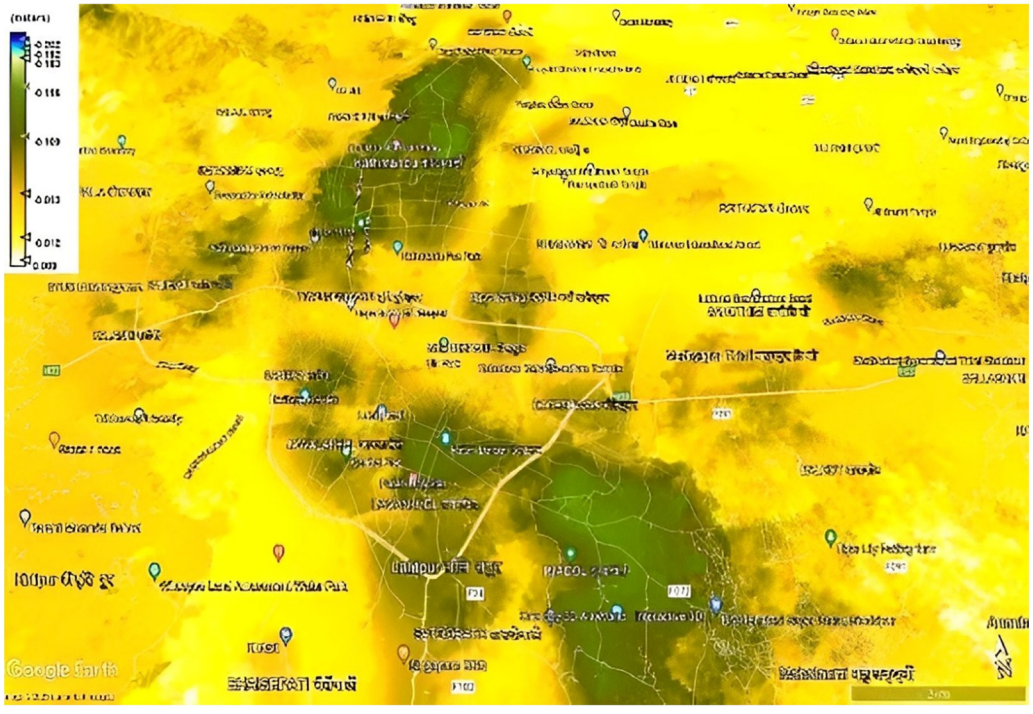

Fig. 6: Map of ground displacement over Kathmandu Valley in the year 2020-2021. The white and yellow part represents maximum ground upliftment and blue and dark green represents subsidence.

The 2020-2021 interferogram as seen in Fig. 6 exhibits a clear intensification of negative LOS displacement compared to the previous year. Central Kathmandu like Thamel deepened to roughly -9 to -12 cm in that interval as seen in Table 2 representing the largest single year negative offsets in our series. The map also shows that previously neutral or slightly uplifted pockets like portions of the northern basin became dominated by subsidence during this step and with a few exceptions such as Budhanilkantha which retained a small positive signal (+0.1 to +0.6 cm). The histogram for 2020-2021 in Fig. 09 right contains almost exclusively downward bars underscoring that this interval was the most uniformly subsiding year in the record. This strong widespread subsidence is plausibly linked to cumulative groundwater draw down in densely developed sectors.

The 2021-2022 interval continued to show negative displacement across the basin as seen in Fig. 7 though the pattern displays subtle spatial differentiation like Budhanilkantha shows the smallest negative magnitude (-2 to -2.5 cm) while Koteshwor and Lagankhel record some of the largest continued subsidence (-5.7 to -5.8 cm). The persistence of subsidence across three consecutive annual intervals indicates either sustained anthropogenic forcing that is ongoing pumping and reduced recharge or longer-term compaction responses in the lacustrine sediments that underlie large portions of the valley's thick compressible sequences as described in Section 2.1 and supported by (Piya et al. 2004). The bar chart for 2021-2022 remains dominated by negative values as shown in Fig.10 left confirming the multi-year nature of the downward trend.

The 2022-2023 map as seen in Fig. 8 shows a striking reversal and most previously subsiding zones display positive LOS motion relative to the previous epoch. Representative values in Table 2 indicate pronounced uplift in several northern and northeastern localities like Budhanilkantha, Jorpati and Tokha each show +11 to +13 cm for this interval while central sites exhibit modest positive changes like Thamel +0.3 to +1.0 cm. The bar chart for 2022-2023 as seen in Fig.10 right shows upward bars across the majority of sampled locations. Such a rapid basin scale rebound across one year suggests a significant hydrological change like enhanced aquifer recharge during monsoon, reduced pumping, or a combination and because elastic recovery following reduced draw down can produce uplift when groundwater pressure partially restores. The magnitude of uplift at Budhanilkantha and Tokha is notable and merits local hydrogeological follow-up. The magnitude of uplift at Budhanilkantha and Tokha is notable and merits local hydrogeological follow-up.

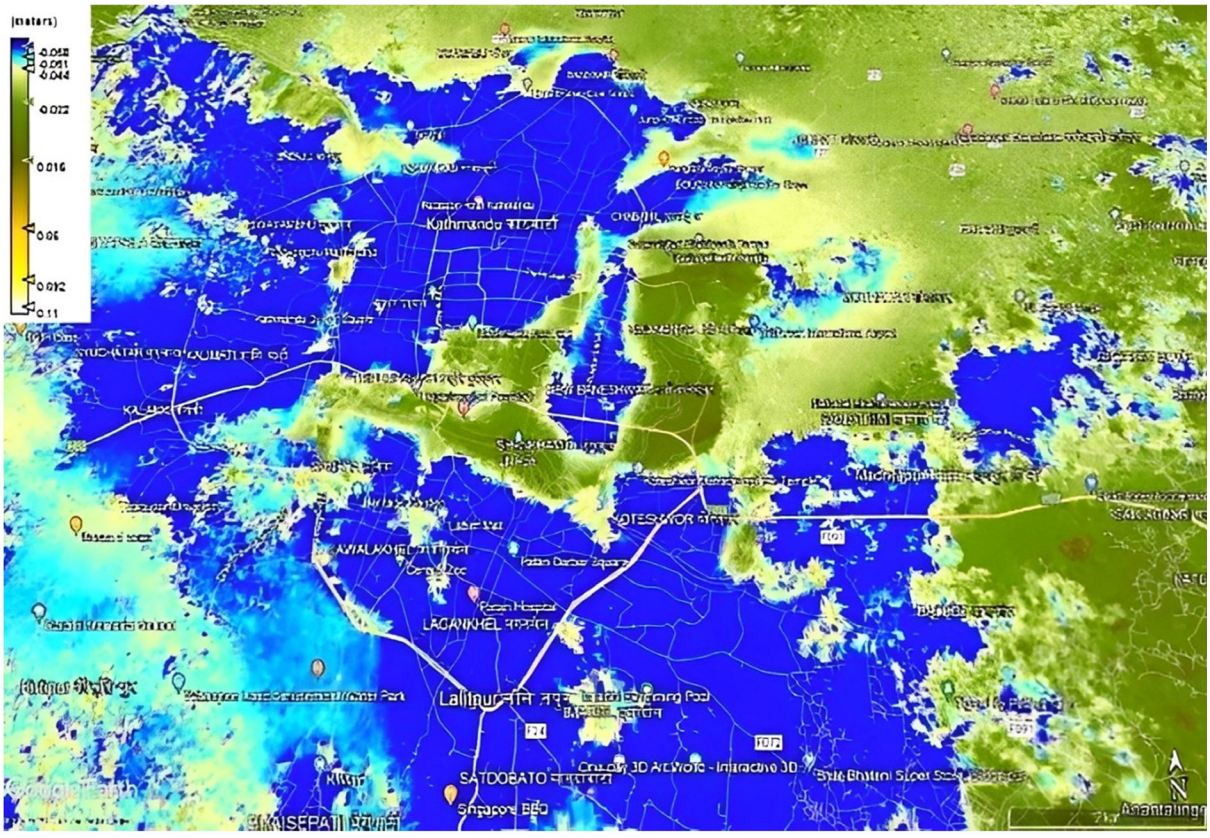

Fig. 7: Map of ground displacement over Kathmandu Valley in the year 2021-2022. The white and yellow part represents maximum ground upliftment and blue and light blue represents subsidence.

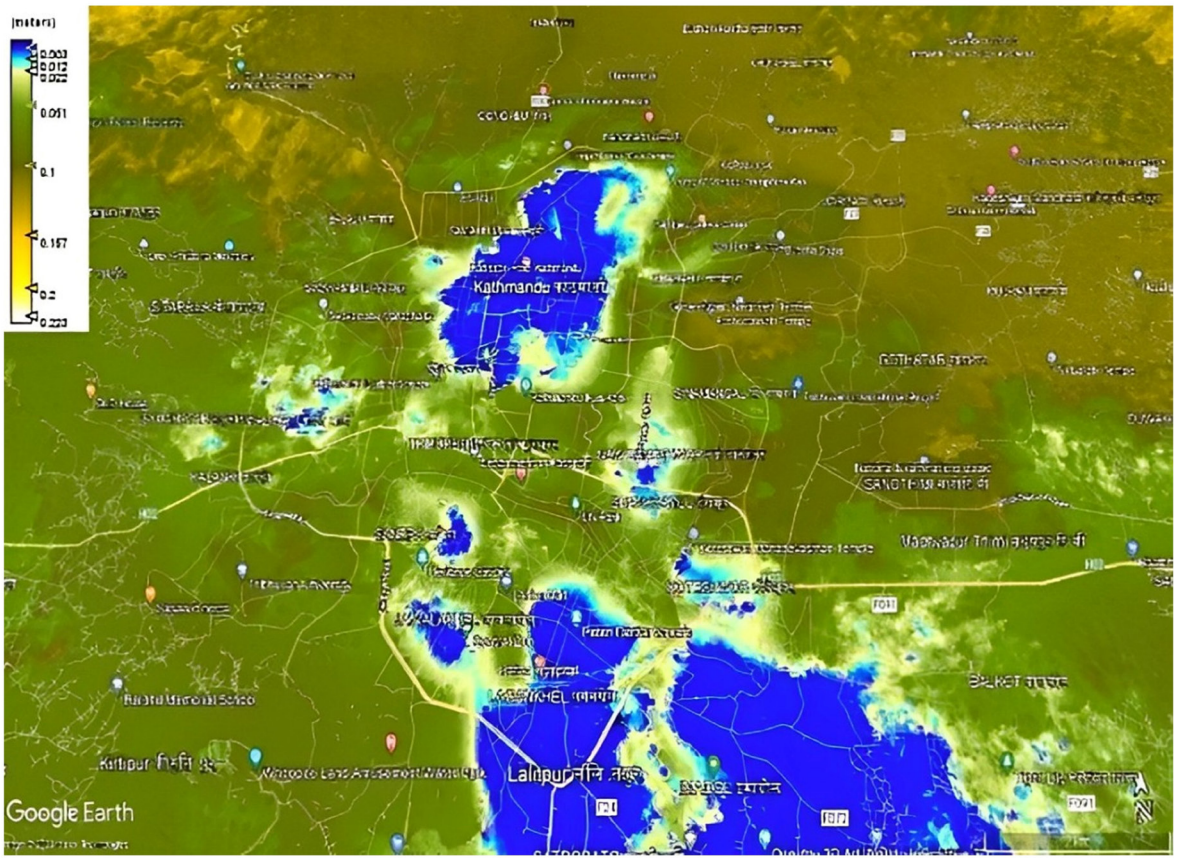

Fig. 8: Map of ground displacement over Kathmandu Valley in the year 2022-2023. The white and yellow part represents maximum ground upliftment and blue and light blue represents minimum upliftment.

Table 2: Annual ground deformation from 2019 to 2023. A negative (-) sign indicates surface subsidence.

Name of Place	Ground displacement (cm) in the years			
	2019-2020	2020-2021	2021-2022	2022-2023
Thamel	-(5.5 - 8.5)	-(9 - 12)	-(5.5 - 5.8)	(0.3 - 1)
Dillibazar	-(4 - 7)	-(5 - 8)	-(5.5 - 5.8)	(0.8 - 1.5)
New Baneshwor	-(4 - 8)	-(6 - 10)	-(4.4 - 5.7)	(0.3 - 2)
Maitighar	-(3 - 5)	-(2 - 5)	-(3.3 - 5.3)	(2.5 - 5)
Balaju	-(2 - 6)	-(2.5 - 4.5)	-(5.4 - 5.8)	(5 - 11)
Gangabu	-(3 - 7)	-(1 - 3)	-(3.4 - 4.4)	(9 - 11)
Budhanilkhantha	(1 - 4)	(0.1 - 0.6)	-(2 - 2.5)	(11 - 13)
Jorpati	(2 - 5)	-(0.1 - 2)	-(3 - 4.8)	(11 - 13)
Boudha	(1 - 3)	-(1.5 - 3)	-(5 - 5.6)	(5 - 7)
Tribhuwan.I. Airport	(0.5 - 2)	-(2 - 5.5)	-(2 - 5.3)	(7 - 10)
Madyapur Timi	-(4 - 6)	-(3 - 6)	-(2 - 5.5)	(5 - 8)
Koteshwor	-(4 - 7)	-(6.5 - 9)	-(5.7 - 5.8)	(0.5 - 2)
Satdobato	-(5 - 7)	-(4 - 6)	-(5.5 - 5.8)	(0.3 - 1.5)
Lagankhel	-(2 - 5)	-(6.5 - 8.5)	-(5.7 - 5.8)	(0.3 - 0.9)
Bhaisepati	-(1 - 4)	-(4.5 - 7)	-(4.5 - 5.8)	(2 - 4)
Kritipur	(4 - 8)	-(4 - 6.5)	-(4.5 - 5.6)	(7 - 9)
Swoyambhu	-(2 - 5)	-(2.5 - 4.5)	-(5.2 - 5.8)	(0.2 - 4)
Kalanki	-(1 - 4)	-(4 - 7.5)	-(5.2 - 5.8)	(5.5 - 7)
Tokha	(0.9 - 2)	-(0.5 - 2.5)	-(2 - 3.5)	(11 - 13)
Imadol	-(3 - 6)	-(8 - 13)	-(4.8 - 5.8)	(0.3 - 0.9)
Khokona	(3 - 7)	-(0.1 - 3.5)	-(4 - 5.5)	(6 - 8)
Jawalakhel	-(3 - 6)	-(6 - 8)	-(4.4 - 5.8)	(0.8 - 2)
Gausala	(3 - 5.5)	-(1 - 3)	-(1.5 - 4.4)	(10 - 12)

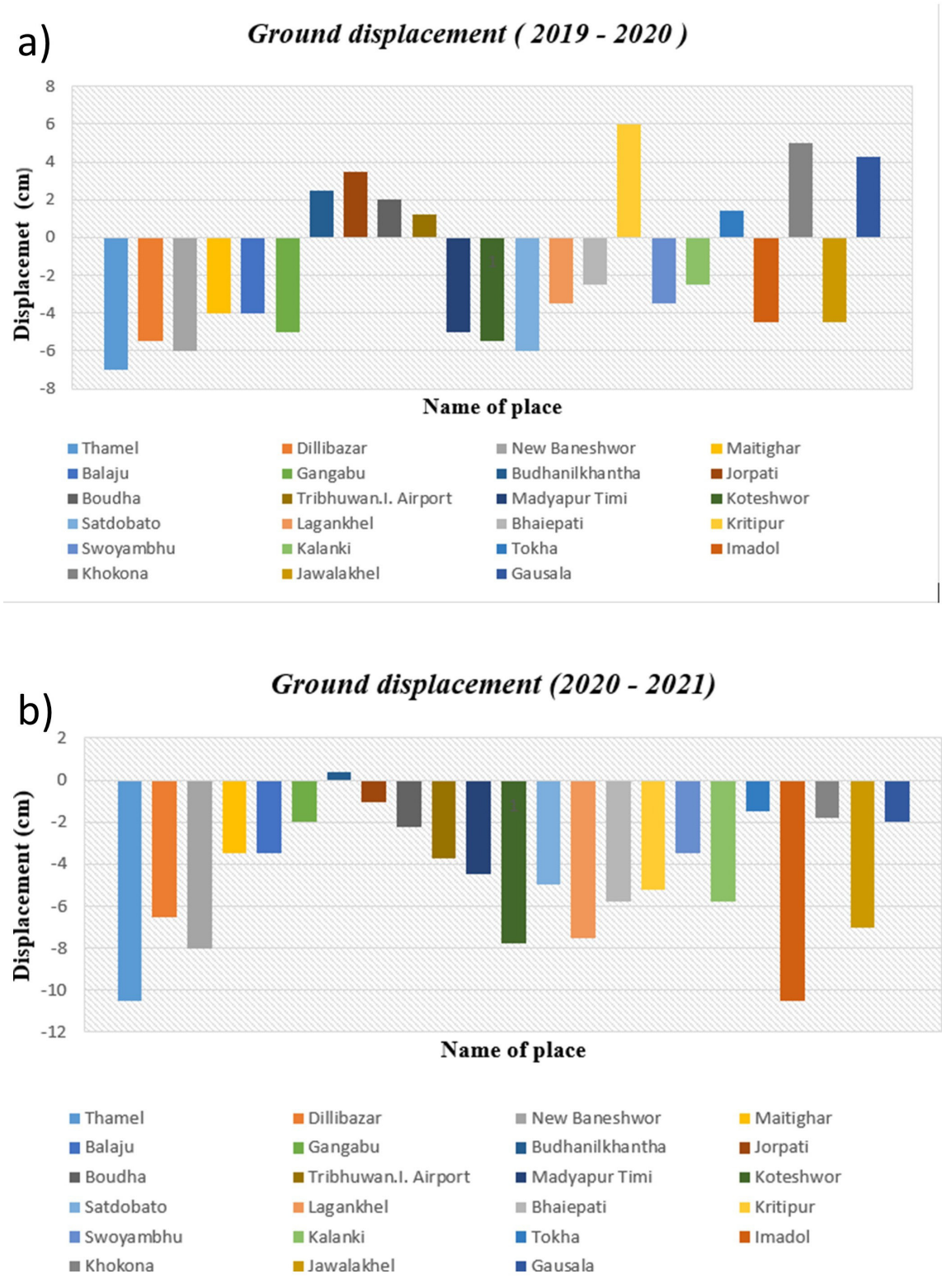

Fig.9: Ground displacement for (2019 - 2020) left and (2020-2021) right along with the name of place indicated with different colors.

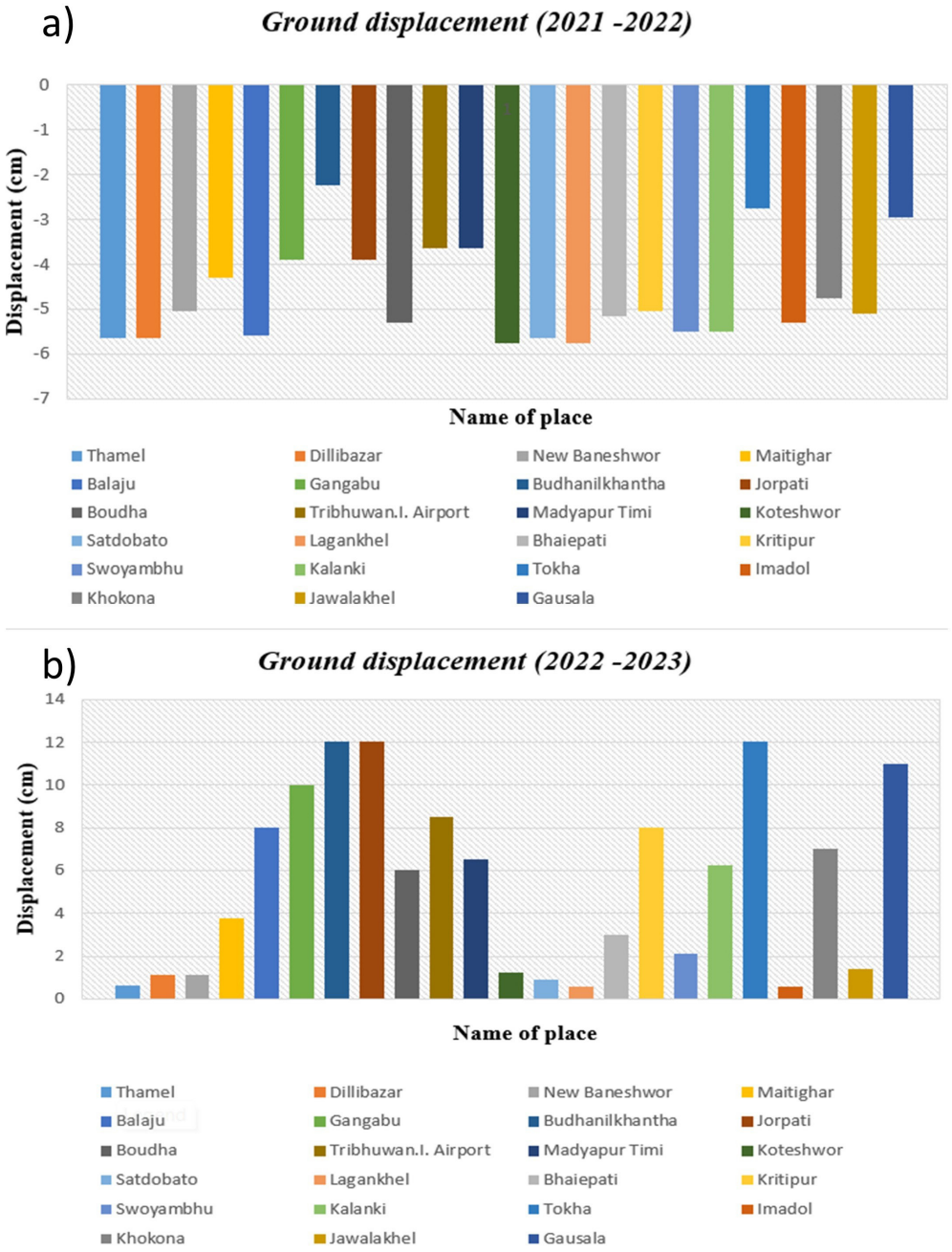

Fig.10: Ground displacement for (2021 - 2022) left and (2022-2023) right along with the name of place indicated with different colors.

Table 3: Average value calculated for different place from Table 2

Name of Place	Year			
	2020	2021	2022	2023
Thamel	-7	-11	-5.65	0.65
New Baneshwor	-6	-8	-5.05	1.15
Budhanilkhantha	2.5	0.35	2.25	12
Tribhuwan.I. Airport	1.25	-3.75	-3.65	8.5
Madyapur Timi	-5	-4.5	-3.75	6.5
Lagankhel	-3.5	-7.5	-5.75	0.6
Kalanki	-2.5	-5.75	-5.5	6.25
Jawalakhel	-4.5	-7	-5.1	1.4

We can see the instability of ground surface from the line graph mentioned below:

The site level line graphs as plotted in the Fig. 11 summarize multiyear cumulative behavior by averaging the annual ranges reported in Table 2 for each monitored locality. These time-series show that for many central sites like Thamel, New Baneshwor, Lagankhel shows cumulative displacement became increasingly negative through 2020-2022 and then moved upward in 2023 reducing the net negative budget. For example, Thamel's mean sequence (-7 cm in 2020, -11 cm in 2021, -5.65 cm in 2022, +0.65 cm in 2023) shows how the 2023 uplift partially offsets prior loss. The graphs are carefully interpreted in the manuscript to note that the plotted lines represent relative changes between annual epochs (not absolute ground elevation) and that cumulative sums across intervals describe net change from the initial reference epoch. These series highlight both the rate and direction changes that are central to understanding hazard implications and aquifer response times.

When the displacement maps are overlaid on urban density and borehole distribution as illustrated in Fig. 1 and discussed in Section 2.1 the strongest subsidence corresponds to areas of dense urbanization and historical intensive pumping like central Kathmandu sectors. Conversely, the uplifted areas in 2022-2023 cluster near zones with either fewer abstraction points or where local recharge might be stronger. This spatial correspondence supports the interpretation that anthropogenic groundwater extraction is a dominant control on the observed multi annual subsidence while year-to-year hydrological variability can drive partial rebound. The research work therefore frames the observed deformation as a coupled tectono-hydrological problem rather than a single cause phenomenon.

We note several important aspects in interpreting these plots like residual atmospheric delay, temporal decorrelation or unmodeled orbital errors can locally bias LOS estimates despite standard SNAP filtering and phase-unwrapping and these sources of uncertainty are discussed in Section 2.3 and were mitigated through multi-look filtering and DEM removal but cannot be entirely eliminated. Additionally, the annual single-pair approach used here provides a first order quantification of year-to-year change but ignores intra annual variability that a time-series SBAS/PSInSAR analysis would better resolve. For this reason, we recommend follow up work using denser time series (SBAS) and integration with groundwater level records and GPS measurements to quantify the elastic vs. inelastic components of the signal. Despite these uncertainties the maps and graphs collectively demonstrate a clear and robust pattern of multiyear subsidence followed by a marked uplift in 2022-2023 that should inform local water management and urban planning decisions.

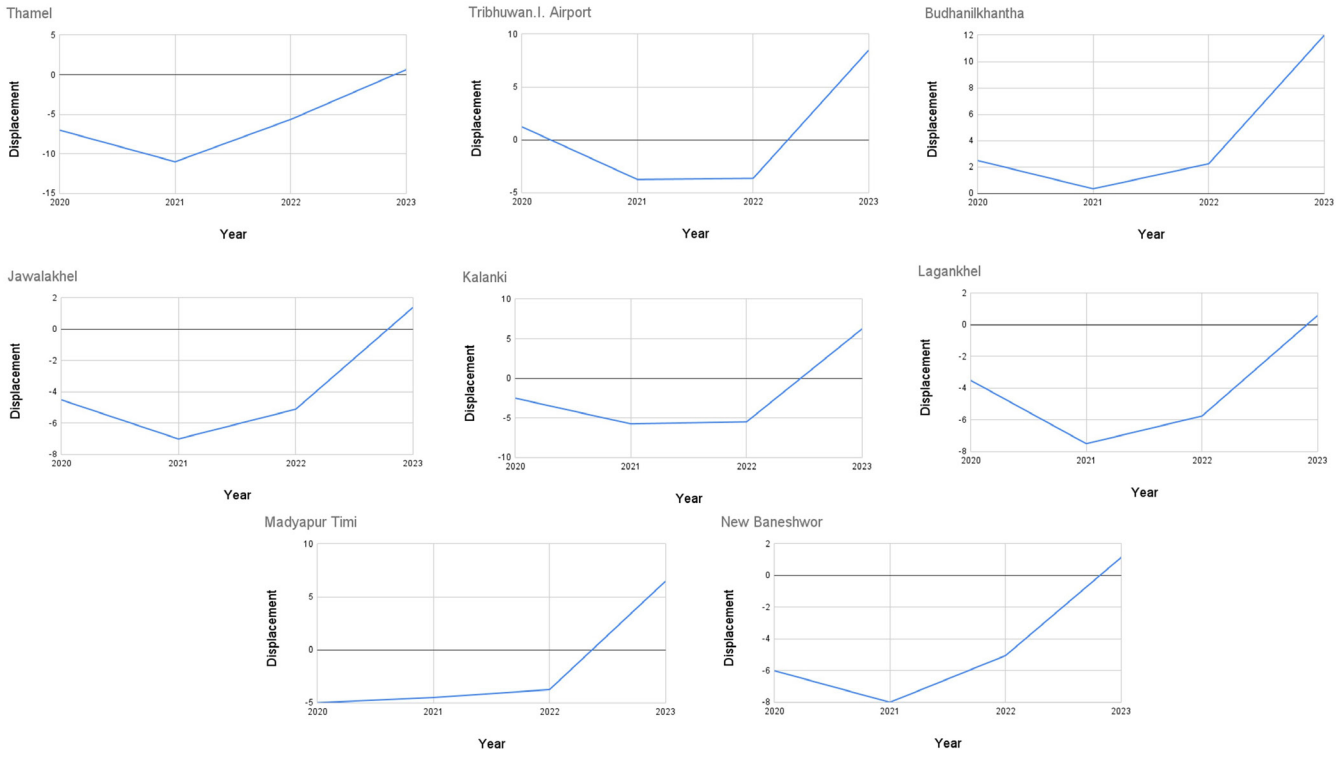

Fig. 11: Line graph of ground displacement of Kathmandu valley of different place.

DISCUSSION

InSAR results indicate clear trends in Kathmandu's surface deformation over 2019-2023. From 2020 through 2022 nearly all parts of the valley were sinking (Table 2) consistent with the known effects of intensive groundwater pumping in a compressible basin. The largest subsidence occurred in the most built up and high demand areas (central Kathmandu) where numerous deep wells have long lowered the water table. (Holzer and Galloway, 2005; Huang et al. 2024; V. P. Pandey et al. 2012) and others have noted that the central and southwestern sectors being highly urbanized with many industrial and municipal wells coincide with observed subsidence hot spots. In our study, Thamel and neighboring central areas subsided the most (10-12 cm per year) while peripheral sites with fewer wells subsided less or even rose slightly when pumping was relaxed. This matches expectations for an aquifer system and large draw down leads to clay compaction and surface lowering. Notably, the northern area of Budhanilkantha showed uplift in the early years and only modest subsidence reflecting both its distance from central pumping centers and possibly local recharge effects.

The shift to net uplift in 2023 suggests a change in conditions. Possible causes include seasonal aquifer recharge like heavy monsoon rains or reduced extraction allowing some elastic rebound of the ground. While Kathmandu has no large reservoir to raise groundwater stricter regulation of pumping or incidental recharge during wet years could partly restore water pressures. Alternatively, long term tectonic strain might have locally pushed the basin floor upward but with no major earthquake in this interval we attribute most of the uplift to hydrological factors. In any case, a 13 cm uplift over one year is unusually large for passive rebound alone so groundwater dynamics are likely dominant.

Our findings are broadly consistent with prior studies. (Bhattarai et al. 2017) used L-band InSAR (ALOS PALSAR) and reported on the order of 10-20 cm of cumulative subsidence in central Kathmandu over 2007-2010 attributing it to 100 m of water table drop. Their map showed the central/southern basin subsiding and the northern basin relatively stable. Similarly, (Huang et al. 2024) recently reported accelerated subsidence (several cm/yr) in Kathmandu using Sentinel-1 time-series highlighting the role of rapid urbanization. By comparison, the 2015 Gorkha earthquake produced much larger displacements (up to 40 cm) in Kathmandu our multi-year magnitudes (11 cm max) are smaller but still significant for infrastructure.

These results underline that Kathmandu is a high deformation zone. Thick lacustrine sediments underlie the city (Sakai, 2001) so any change in stress tectonic or hydrologic can translate to meters of subsurface deformation. The combination of Himalayan tectonics and human impact is key as (Saji et al. 2020) noted global subsidence is often driven by groundwater withdrawal in combination with urban land use changes. In Kathmandu's case we have documented exactly this heavy pumping in newly urbanized areas is causing the basin to sink while reduced stress in 2023 allowed uplift. These deformation rates (cm per year) pose risks and uneven settling can crack foundations, tilt buildings and disrupt road and pipeline networks.

Continued monitoring is vital for the development of the city. The clear annual signal we observe demonstrates that InSAR can detect Kathmandu's deformation reliably. Urban planners and water managers should consider these results for example targeted restrictions on pumping in critical areas could slow subsidence. Engineering designs like foundations should account for the possibility of several centimeters of movement over a few years. Finally, future research should link these deformation maps to detailed hydrological models to predict how changes in extraction or recharge will affect the land surface.

CONCLUSIONS

In this research, the prevalence of ground deformation in the Kathmandu Valley was discovered using (InSAR). We used one day of a year to compare the deformation of the valley. We have used almost one year interval time to calculate the surface deformation and also a four-year interval time. The following results can be found from this research:

1. Kathmandu Valley's ground is actively moving. Our InSAR analysis shows pronounced subsidence during 2020-2022 and net uplift in 2023 indicating an unstable subsurface.
2. The greatest downward movement occurred in the central and southern basin (Thamel, Baneshwor, Lagankhel) whereas northern areas (Budhanilkantha, Jorpati, Tokha) exhibited uplift in 2023.
3. These trends are attributable to human and natural causes. Intensive groundwater extraction in populated zones likely drove the 2020-2022 subsidence. The observed uplift in 2023 suggests partial recharge or reduced pumping. Tectonic loading (India-Eurasia convergence) provides a long-term upward push though its signature here is modest.
4. We measured up to 12 cm annual subsidence (peak at Thamel 2020-21) and +13 cm uplift (Budhanilkantha 2022-23). These values while smaller than 2015 earthquake offsets are large enough to affect infrastructure in short term.
5. Given the valley's high deformation potential (deep sediments and growing population) we urge authorities to manage groundwater sustainably. Building codes should include allowance for differential settlement. We also recommend establishing regular InSAR-based monitoring as an early warning system.

In summary, this study confirms that Kathmandu Valley remains a subsidence prone region with deformation linked to both tectonic setting and unsustainable aquifer use. Timely policy action on water management and urban planning will be crucial to mitigate the risks revealed by our InSAR observations.

ACKNOWLEDGMENT

The authors acknowledge their gratitude to European Space Agency (ESA) for providing the SNAP toolkit for data processing, which was heavily utilized in this work, and for

free access to Sentinel-1A SAR satellite datasets. The authors would also like to thank the Department of Physics, St. Xavier's College for providing their support.

Declaration of interest: The authors declare that they have no financial interests or personal relationships that have appeared in this paper.

REFERENCE

Bajracharya, A., Pradhan, P., Amatya, P., Khokhali, B. B., Shrestha, S., and Hasan, A., 2015, Planning for affordable housing during densification in Kathmandu: Lessons from four settlements. International Institute for Environment and Development. https://www.jstor.org/stable/resrep01315.

Bhattarai, R., Alifu, H., Maitiniyazi, A., and Kondoh, A., 2017, Detection of Land Subsidence in Kathmandu Valley, Nepal, Using DInSAR Technique. Land, v. 6(2), pp. 39. https://doi.org/10.3390/land6020039.

Castellazzi, P., Arroyo-Domínguez, N., Martel, R., Calderhead, A. I., Normand, J. C. L., Gárfias, J., and Rivera, A., 2016, Land subsidence in major cities of Central Mexico: Interpreting InSAR-derived land subsidence mapping with hydrogeological data. International Journal of Applied Earth Observation and Geoinformation, v. 47, pp. 102–111. https://doi.org/10.1016/j.jag.2015.12.002.

Chapagain, D. P., 2013, Urban Water Supply Sector Reform in Kathmandu Valley. Journal of the Institute of Engineering, v. 9(1), pp. 130–141. https://doi.org/10.3126/jie.v9i1.10678.

Du, Q., Li, G., Chen, D., Zhou, Y., Qi, S., Wu, G., Chai, M., Tang, L., Jia, H., and Peng, W., 2021, SBAS-InSAR-Based Analysis of Surface Deformation in the Eastern Tianshan Mountains, China. Frontiers in Earth Science, v. 9. https://doi.org/10.3389/feart.2021.729454.

Du, Q., Li, G., Zhou, Y., Chai, M., Chen, D., Qi, S., and Wu, G., 2021, Deformation Monitoring in an Alpine Mining Area in the Tianshan Mountains Based on SBAS-InSAR Technology. Advances in Materials Science and Engineering, v. 2021(1), pp. 9988017. https://doi.org/10.1155/2021/9988017.

Gautam, R., and Rao, G. K., 1991, Groundwater resource evaluation of the Kathmandu valley. Journal of Nepal Geological Society, v. 7, pp. 39–48. https://doi.org/10.3126/jngs.v7i0.32582.

Goda, K., Kiyota, T., Pokhrel, R. M., Chiaro, G., Katagiri, T., Sharma, K., and Wilkinson, S. , 2015, The 2015 Gorkha Nepal Earthquake: Insights from Earthquake Damage Survey. Frontiers in Built Environment, v. 1. https://doi.org/10.3389/fbuil.2015.00008.

Holzer, T. L., and Galloway, D. L., 2005, Impacts of land subsidence caused by withdrawal of underground fluids in the United States. In J. Ehlen, W. C. Haneberg, and R. A. Larson (Eds.), Humans as Geologic Agents, Geological Society of America, v. 16. https://doi.org/10.1130/2005.4016(08)

Huang, J., Sinclair, H., Pokhrel, P., and Watson, C. S., 2024, Rapid subsidence in the Kathmandu Valley recorded using Sentinel-1 InSAR. International Journal of Remote Sensing, v. 45(1), pp. 1–20. https://doi.org/10.1080/01431161.2023.2283902.

Kumar, A., Manisha, Lal, P., Prasad, A., Tripathy, P., and Saikia, P., 2022, Analyzing urban damage and surface deformation based hazard-risk in Kathmandu city occurred during Nepal earthquake (2015) using SAR interferometry. Advances in Space Research, v. 70(12), pp. 3892–3904. https://doi.org/10.1016/j.asr.2022.02.003.

Moribayashi, S., and Maruo, Y., 1980, Basement Topography of the Kathmandu Valley, Nepal. Journal of the Japan Society of Engineering Geology, v. 21(2), pp. 80–87. https://doi.org/10.5110/jjseg.21.80.

Pandey, M. R., 2000, Ground response of Kathmandu Valley on the basis of microtremors. Proceedings of the 12th World Conference on Earthquake Engineering.

Pandey, M. R., Tandukar, R. P., Avouac, J. P., Vergne, J., and Héritier, T., 1999, Seismotectonics of the Nepal Himalaya from a local seismic network. Journal of Asian Earth Sciences, v. 17(5), pp. 703–712. https://doi.org/10.1016/S1367-9120(99)00034-6.

Pandey, V. P., Shrestha, S., and Kazama, F., 2012, Groundwater in the Kathmandu Valley: Development dynamics, consequences and prospects for sustainable management. European Water, v. 34, pp. 3–14.

Pepe, A., and Calò, F. ,2017, A Review of Interferometric Synthetic Aperture RADAR (InSAR) Multi-Track Approaches for the Retrieval of Earth's Surface Displacements. Applied Sciences, v. 7(12), pp. 1264. https://doi.org/10.3390/app7121264.

Piya, B., Westen, C. van, and Woldai, T. (2004). Geological database for liquefaction hazard analysis in the Kathmandu valley, Nepal. Journal of Nepal Geological Society, v. 30, pp. 141–152. https://doi.org/10.3126/jngs.v30i0.31704.

Saji, A. P., Sunil, P. S., Sreejith, K. M., Gautam, P. K., Kumar, K. V., Ponraj, M., Amirtharaj, S., Shaju, R. M., Begum, S. K., Reddy, C. D., and Ramesh, D. S., 2020, Surface Deformation and Influence of Hydrological Mass Over Himalaya and North India Revealed From a Decade of Continuous GPS and GRACE Observations. Journal of Geophysical Research: Earth Surface, v. 125(1), pp. e2018JF004943. https://doi.org/10.1029/2018JF004943.

Sakai, H., 2001, Stratigraphic division and sedimentary facies of the Kathmandu Basin Group, central Nepal. Journal of Nepal Geological Society, v. 25, pp. 19–32. https://doi.org/10.3126/jngs.v25i0.32043.

Stramondo, S., Bozzano, F., Marra, F., Wegmuller, U., Cinti, F. R., Moro, M., and Saroli, M. ,2008, Subsidence induced by urbanisation in the city of Rome detected by advanced InSAR technique and geotechnical investigations. Remote Sensing of Environment, v. 112(6), pp. 3160–3172. https://doi.org/10.1016/j.rse.2008.03.008.

Subedi, M., KC, R., and Acharya, I., 2021, SPT-based seismic soil liquefaction potential evaluation of Kathmandu Valley using first-order second-moment method.

Taylor, R. G. et al., 2013, Ground water and climate change. Nature Climate Change, v. 3(4), pp. 322–329. https://doi.org/10.1038/nclimate1744.

Wang, Y., Guo, Y., Hu, S., Li, Y., Wang, J., Liu, X., and Wang, L. , 2019, Ground Deformation Analysis Using InSAR and Backpropagation Prediction with Influencing Factors in Erhai Region, China. Sustainability, v. 11(10), pp. 2853. https://doi.org/10.3390/su11102853.

Yulianto, S., Anisah, A., Agustan, A., Sumargana, L., Anantasena, Y., and Santosa, B. H., 2021. Spatial Distribution of Paddy Growth Stage Using Sentinel-1 based on CART Model. 2021 IEEE Asia-Pacific Conference on Geoscience, Electronics and Remote Sensing Technology (AGERS). https://doi.org/10.1109/AGERS53903.2021.9617317.

Zhang, Z., Wang, X., Wu, Y., Zhao, Z., and E, Y. ,2021,. Applied Research on InSAR and GPS Data Fusion in Deformation Monitoring. Scientific Programming, v. 2021(1), pp. 3888975. https://doi.org/10.1155/2021/3888975.